Control and Optimization of a Wind Energy Conversion System Based on Doubly-Fed Induction Generator Using Nonlinear Control Strategies

Mohammed Fdaili *‡, Ahmed Essadki *, Mohamed Nadour *, Tamou Nasser **,

* Research Center in Sciences and Technologies of Engineering and Health (STIS), Laboratory of Electrical Engineering (LEG), Higher Normal School of Technical Education (ENSET), Mohammed V University Rabat, Morocco.

** Laboratory of embedded systems engineering, Higher National School of Computer Science and Systems Analysis, Mohammed V University Rabat, Morocco.

(mohamed.fdaili@um5s.net.ma, ahmed.essadki1@gmail.com, mohamed.nadour@um5s.net.ma, tnasser@ensias.ma)

‡ Corresponding Author; Mohammed Fdaili, Tel: +2126 6099 5478, mohamed.fdaili@um5s.net.ma

Received: 29.11.2018 Accepted: 28.12.2018

Abstract- Classical vector control schemes use proportional-integral (PI) controllers for wind energy conversion system (WECS) based on doubly-fed induction generator (DFIG) present many drawbacks and limitations, such as sensibility to DFIG's parameter variations, parameter adjustment difficulties and less robust against the external and internal disturbances. Therefore, and to overcome these inconveniences, nonlinear control strategies of the DFIG-model will be more appropriate to ensure better results than that of the PI controllers. In this paper, three control techniques: fuzzy-sliding mode (FSMC), second-order sliding mode (SOSMC) and integral backstepping (IBSC) for both the rotor side converter (RSC) and the grid side converter (GSC), using a pulse width modulation (PWM) with fixed switching frequency, of the whole WECS are presented and designed. The principal purpose of proposed control strategies is to extract the maximum power (MPPT) and keeping a stable operation of a DFIG and its converters during internal and external uncertainties. The overall results are afforded by simulation in the SIMULINK/MATLAB software. Simulation results exposed in this work demonstrate the robustness of each control strategy in spite of the different disturbances and uncertainties.

Keywords Maximum power point tracking (MPPT), Wind Energy Conversion System (WECS), DFIG, Fuzzy-sliding mode, Second order sliding mode, Integral backstepping.

Nomenclatures

Ω_m	Mechanical speed (rad/s)	ω	Angular speed (rad/s)
s	Stator axes index	T	Torque component (N.m)
r	Rotor axes index	P	Active power component (W)
f	Filter axes index	Q	Reactive power component (VAR)
g	Grid axes index	ψ	Flux component (Wb)
d	Direct axes	i	Current component (A)
q	Quadrature axes	v	Voltage component (V)

1. Introduction

Generally, the performances of WECS equipped with DFIG technology repose on the control techniques applied on turbine and DFIG, which are mostly designed by a cascaded structure that contains a slow speed regulator of turbine subsystem and a fast power regulation of DFIG subsystem. WTSs are usually equipped with the MPPT strategy to extract the maximum power from the available kinetic energy [1, 2, 3, 4, 5]. This technique consists of varying the reference speed of the machine according to that of the wind [1]. In addition, the pitch angle control was employed to limit the output mechanical power when wind speed above the rated value [2]. Therefore, the aim of these control systems is to maximize the extraction of captured energy, and also to protect the WTS from overloading.

Classical sliding mode control (SMC), which called also first-order SMC, has been extensively used in many applications in recent decades [2, 6], such as the power regulation of DFIG based WECS. SMC is a powerful control approach with an effective rejection of disturbances and uncertainties, strong robustness against parameter variations and fast response [2, 6]. Therefore, it is appropriate to avoid the limitation of PI controllers. Despite all that, SMC still has one major inconvenience that may impact its extent of use, which is the chattering phenomenon produced by the discontinuous component of control law. To mitigate this problem, different modifications to the classical SMC law have been proposed. In this paper, FSM control methodology (fuzzy logic in combination with sliding mode, as depicted in [6, 7, 8]) is introduced as a first solution to tackle the previous hurdle. Secondly, SOSM control is proposed to limit the above problem and to preserve the principal advantages of the classical SMC approach, such as its simplicity, robustness and convergence of sliding variables to zero in finite time, as presented in [2, 9].

The SOSM control approach is extensively suggested for 2-order uncertain plants by the use of a discontinuous component acting on the second derivative of the constraint function [9]. Furthermore, this control technique guarantees the same static/dynamic performances and robustness of first-order SMC strategy, and also, at the same time, reduces the chattering phenomenon [2, 6, 7, 9]. Finally, as a third solution, IBS control strategy is proposed to achieve high performances of the WECS.

In the context of trajectory pursuit, the basic idea of backstepping control is to make the looped system equivalent to stable cascaded first-order subsystems [3, 2]. It allows to determining the system control law by the proper choice of the Lyapunov function, as demonstrated in [3, 10]. This technique permits a robust control law synthesis despite the DFIG parameter variations and certain disturbances. Moreover, in order to furthermore ameliorate the classical backstepping control (BSC) approach robustness, an integral term is introduced in combination with the BSC forming the integral backstepping controller (IBSC) [11]. The control parameters of the IBSC approach, if correctly chosen, guarantee the elimination of the steady-state error that characterizes many control strategies in presence of parameter variations, uncertainties and disturbances.

The rest of this paper is organized as follows: In section 2, a description of the overall system studied shown in Fig. 1 is briefly presented. The FSM, SOSM and IBS control approaches are applied in section 3 and section 4. The simulation results are illustrated in section 5 and 6. Finally, some conclusions are summarized in section 7.

2. Modeling of wind turbine conversion system (WTCS)

A simple description of the overall scheme of the grid-connected WTCS is illustrated in Fig. 1.

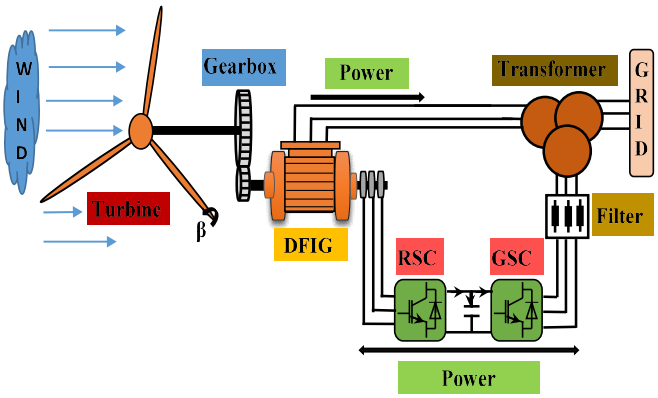

Fig. 1. WECS generation structure.

2.1. DFIG modeling

Let's recall the equations system characterizing the DFIG model, which are written in the Park reference frame, as elaborated in the literature [2, 4, 5, 9, 12, 13, 14].

$$\begin{cases} v_{sd} = R_s.i_{sd} + \dfrac{d\psi_{sd}}{dt} - \omega_s.\psi_{sq} \\ v_{sq} = R_s.i_{sq} + \dfrac{d\psi_{sq}}{dt} + \omega_s.\psi_{sd} \\ v_{rd} = R_r.i_{rd} + \dfrac{d\psi_{rd}}{dt} - \omega_r.\psi_{rq} \\ v_{rq} = R_r.i_{rq} + \dfrac{d\psi_{rq}}{dt} + \omega_r.\psi_{rd} \end{cases}, \begin{cases} \psi_{sd} = L_s.i_{sd} + M.i_{rd} \\ \psi_{sq} = L_s.i_{sq} + M.i_{rq} \\ \psi_{rd} = L_r.i_{rd} + M.i_{sd} \\ \psi_{rq} = L_r.i_{rq} + M.i_{sq} \end{cases} \quad (1)$$

The DFIG model is completed by the Eq. (2) [15].

$$\begin{cases} T_{gr} = T_{em} + J.\dfrac{d\Omega_m}{dt} + D.\Omega_m \\ T_{em} = p.\left(\Psi_{sd}.i_{sq} - \Psi_{sq}.i_{sd}\right) \end{cases} \quad (2)$$

In SFO, the d-axis is fixed to the stator flux. Thus, $\Psi_{sq} = 0$ and $\Psi_{sd} = \Psi_s$. Based on these assumptions, the electrical equations can be re-written as follows:

$$\begin{cases} v_{sd} = \dfrac{R_s}{L_s}\cdot\Psi_{sd} + \dfrac{R_s.M}{L_s}\cdot i_{rd} + \dfrac{d\Psi_{sd}}{dt} \\ v_{rd} = \sigma.L_r\left(\dfrac{di_{rd}}{dt} + \alpha\cdot i_{rd} - \beta\cdot R_s\cdot\Psi_{sd} + \gamma\cdot v_{sd} - w_r\cdot i_{rq}\right) \\ v_{rq} = \sigma.L_r\left(\dfrac{di_{rq}}{dt} + \delta\cdot i_{rq} + \gamma\cdot w_r\cdot\Psi_{sd} + w_r\cdot i_{rd}\right) \\ T_{em} = -\mu.i_{rq}.\Psi_{sd} \end{cases} \quad (3)$$

Where: $\begin{cases} \sigma = 1 - \dfrac{M^2}{L_s.L_r}, \delta = \dfrac{R_r}{\sigma.L_r} \\ \alpha = \dfrac{R_r.L_s^2 + R_s.M^2}{\sigma.L_r.L_s^2}, \mu = p\cdot\dfrac{M}{L_s} \\ \beta = \dfrac{M}{\sigma.L_r.L_s^2}, \gamma = \dfrac{M}{\sigma.L_r.L_s} \end{cases}$

2.2. DC-link modeling

The continuous bus (DC) between the GSC and the RSC is represented by a pure capacitance (C); the voltage of DC-link is expressed as follows:

$$\begin{cases} U_{dc} = \dfrac{1}{C}\cdot\int_0^t \left(i_{rm}(\tau) - i_{gm}(\tau)\right)d\tau \\ P_c = U_{dc}.\mathrm{i}_c \\ P_g = P_r - P_c = U_{dc}.\mathrm{i}_{gm} \\ P_r = U_{dc}.\mathrm{i}_{rm} \end{cases} \quad (4)$$

2.3. Filter and Grid modeling

The RL-filter model is described by the following equation:

$$\begin{cases} v_{fd} = R_f.\mathrm{i}_{fd} + L_f.\dfrac{d\,\mathrm{i}_{fd}}{dt} - w_s.\mathrm{L}_f.\mathrm{i}_{fq} \\ v_{fq} = R_f.\mathrm{i}_{fq} + L_f.\dfrac{d\,\mathrm{i}_{fq}}{dt} + w_s.\mathrm{L}_f.\mathrm{i}_{fd} + v_{gq} \\ P_g = v_{gq}.\mathrm{i}_{fq} \\ \mathrm{Q}_g = v_{gq}.\mathrm{i}_{fd} \end{cases} \quad (5)$$

The equations below (Eq. (5)) are obtained by fixing the q-axis of the reference frame to the grid voltage.

3. RSC control strategies

The purpose from controlling the RSC of the WECS is to ensure a decoupled control between the stator active and reactive powers produced by the DFIG, and this, by controlling both d and q rotor current components, as shown in Fig. 2. To do this, three control strategies (FSMC, SOSMC and IBSC) are proposed to control the RSC by controlling the direct and quadrature current components through the control of direct stator flux and electromagnetic torque components.

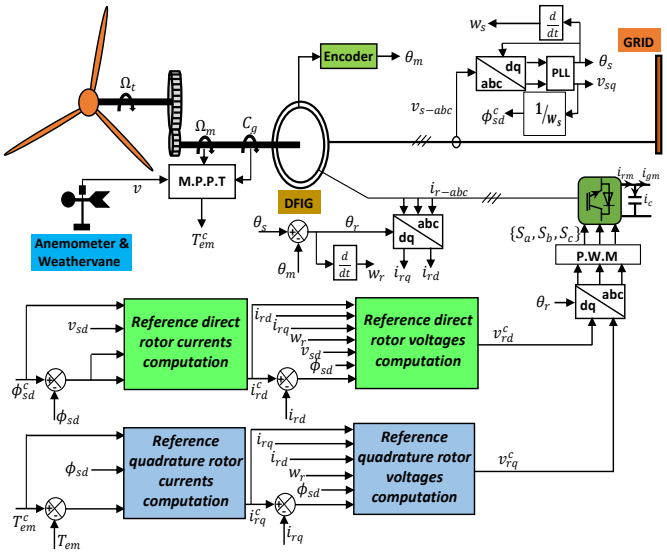

Fig. 2. RSC structure design.

3.1. Fuzzy sliding mode control

The control law of FSM control algorithm is defined as follows:

$$U^c = U^{eq} + U^{fuzzy} \quad (6)$$

- Reference rotor currents computation

By introducing the sliding surface function for the electromagnetic torque (T_{em}) and direct stator flux (Ψ_{sd}), respectively. We can write:

$$\begin{cases} S(T_{em}) = T_{em}^c - T_{em} \\ S(\Psi_{sd}) = \Psi_{sd}^c - \Psi_{sd} \end{cases}, \quad \begin{cases} \dot{S}(T_{em}) = \dot{T}_{em}^c - \dot{T}_{em} \\ \dot{S}(\Psi_{sd}) = \dot{\Psi}_{sd}^c - \dot{\Psi}_{sd} \end{cases} \quad (7)$$

The references of the direct and quadrature rotor currents are obtained by imposing $S(T_{em}) = 0$ and $S(\Psi_{sd}) = 0$ .As a result, we found:

$$\begin{cases} i_{rq}^c = -\dfrac{1}{\mu}\int_0^t \dfrac{\dot{T}_{em}^c}{\psi_{sd}}d\tau + i_{rq}^n \\ i_{rd}^c = \dfrac{L_s}{R_s.M}\cdot\dot{\psi}_{sd}^c - \dfrac{L_s}{R_s.M}\cdot v_{sd} + \dfrac{\psi_{sd}}{M} + i_{rd}^n \end{cases} \quad (8)$$

Where: $\begin{cases} i_{rq}^n = K_{irq}.sign\left(S(T_{em})\right) \\ i_{rd}^n = K_{ird}.sign\left(S(\psi_{sd})\right) \end{cases}$

To achieve the system stability condition, K_{irq} and K_{ird} must be chosen positive. The Lyapunov equation keeps the sliding surface attractive and invariant [2].

The discontinuous control actions (i_{rq}^n & i_{rd}^n) produce a harmful phenomenon, knows as "chattering", which can excite the high-frequencies until the system is damaged. Consequently, the discontinuous control variables have been replaced by a continuous fuzzy logic variables [6, 7]. The Table 1 shows the fuzzy controller inference matrix for a partition of 7 fuzzy sets for each input and output variable. A symmetric triangular membership functions are used on a normalized universe of discourse for each variable as shown in Fig. 3. The inputs of FSM controller, studied in this paper, are the error and its deviation and the output variable is the control signal.

Table 1. Rule matrix for FLCs [6, 7]

		e						
	$i_{rd/q}$	NB	NM	NS	ZE	PS	PM	PB
$\dot{e}$	NB	NB	NB	NB	NB	NM	NS	ZE
	NM	NB	NB	NB	NM	NS	ZE	PS
	NS	NB	NB	NM	NS	ZE	PS	PM
	ZE	NB	NM	NS	ZE	PS	PM	PB
	PS	NM	NS	ZE	PS	PM	PB	PB
	PM	NS	ZE	PS	PM	PB	PB	PB
	PB	ZE	PS	PM	PB	PB	PB	PB

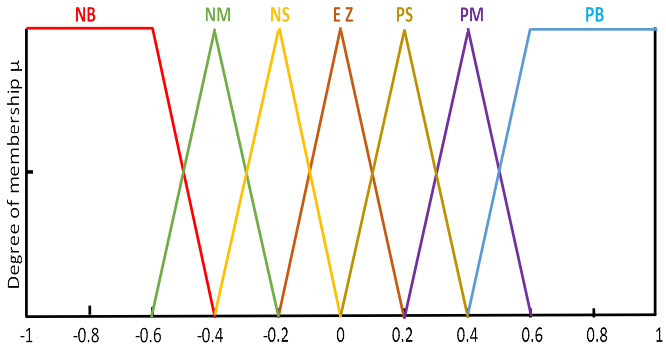

Fig. 3. Membership function for input and output variables.

- Reference rotor voltages computation

The Eq. (9) gives the sliding surface for the direct and quadrature current i_{rd} , i_{rq} , respectively.

$$\begin{cases} S\left(i_{rd}\right)=i_{rd}^{c}-i_{rd} \\ S\left(i_{rq}\right)=i_{rq}^{c}-i_{rq} \end{cases}, \begin{cases} \dot{S}\left(i_{rd}\right)=\dot{i}_{rd}^{c}-\dot{i}_{rd} \\ \dot{S}\left(i_{rq}\right)=\dot{i}_{rq}^{c}-\dot{i}_{rq} \end{cases} \tag{9}$$

The equivalent control terms are obtained when $S\left(i_{rd}/i_{rq}\right)=0$, $\dot{S}\left(i_{rd}/i_{rq}\right)=0$ and $v_{rd}^{n}=v_{rq}^{n}=0$. Consequent-ly, the control voltage components are defined as:

$$\begin{cases} v_{rq}^{c}=\sigma.L_{r}\left(\dot{i}_{rq}^{c}+\delta.i_{rq}+\gamma.w_{r}.\psi_{sd}+w_{r}.i_{rd}\right)+v_{rq}^{fuzzy} \\ v_{rd}^{c}=\sigma.L_{r}\left(\dot{i}_{rd}^{c}+\alpha.i_{rd}-\beta.R_{s}.\psi_{sd}+\gamma.v_{sd}-w_{r}.i_{rq}\right)+v_{rd}^{fuzzy} \end{cases} \tag{10}$$

The fuzzy rules and membership functions used for both the inputs and the output are similar to that presented in Table 1 and Fig. 3, respectively.

3.2. Second order sliding mode control

The proposed control algorithm is based on super-twisting algorithm (STA), which is introduced by Levant [16, 17, 18]. The SOSM controllers contain two components: the equivalent control term and the switching control term.

- Reference rotor currents computation

The switching function which permits to determinate the reference of the currents is selected as shown in Eq. (11).

$$\begin{cases} S\left(T_{em}\right)=T_{em}^{c}-T_{em}+C_{1}\int_{0}^{t}\left(T_{em}^{c}-T_{em}\right)d\tau \\ S\left(\Psi_{sd}\right)=\Psi_{sd}^{c}-\Psi_{sd}+C_{2}\int_{0}^{t}\left(\Psi_{sd}^{c}-\Psi_{sd}\right)d\tau \end{cases} \tag{11}$$

$$\begin{cases} \dot{S}\left(T_{em}\right)=\dot{T}_{em}^{c}-\dot{T}_{em}+C_{1}\left(\dot{T}_{em}^{c}-\dot{T}_{em}\right) \\ \dot{S}\left(\Psi_{sd}\right)=\dot{\Psi}_{sd}^{c}-\dot{\Psi}_{sd}+C_{2}\left(\dot{\Psi}_{sd}^{c}-\dot{\Psi}_{sd}\right) \end{cases} \tag{12}$$

The integral terms are introduced to eliminate the steady-state errors. C_1 and C_2 are positive gains. The equivalent control components (i_{rd}^{eq} & i_{rq}^{eq}) are obtained by imposing: $S\left(T_{em}\right)=0$, $S(\psi_{sd})=0$, $\dot{S}\left(T_{em}\right)=0$ and $\dot{S}(\psi_{sd})=0$. Therefore, the control signals are depicted as follows:

$$\begin{cases} i_{rq}^{c}=-\dfrac{1}{\mu}\int\dfrac{1}{\psi_{sd}}\left(\dot{T}_{em}^{c}+C_{1}\left(T_{em}^{c}-T_{em}\right)\right)+i_{rq}^{ST} \\ i_{rd}^{c}=\dfrac{L_{s}}{R_{s}.M}\cdot\dot{\psi}_{sd}^{c}-\dfrac{L_{s}}{R_{s}.M}\cdot v_{sd}+\dfrac{\psi_{sd}}{M}+\dfrac{L_{s}}{R_{s}.M}C_{2}\left(\psi_{sd}^{c}-\psi_{sd}\right)+i_{rd}^{ST} \end{cases} \tag{13}$$

Basing on the STA proposed by Levant [16, 17, 18], the switching control terms are defined as follows:

$$\begin{cases} i_{rq}^{ST}=K_{irq}^{1}\sqrt{\left|S\left(T_{em}\right)\right|}.sign\left(S\left(T_{em}\right)\right)+K_{irq}^{2}\int_{0}^{t}sign\left(S\left(T_{em}\right)\right)d\tau \\ i_{rd}^{ST}=K_{ird}^{1}\sqrt{\left|S\left(\psi_{sd}\right)\right|}.sign\left(S\left(\psi_{sd}\right)\right)+K_{ird}^{2}\int_{0}^{t}sign\left(S\left(\psi_{sd}\right)\right)d\tau \end{cases} \tag{14}$$

Where, the gains verify the following condition: $K_{irq}^{1},K_{irq}^{2},K_{ird}^{1}$ and K_{ird}^{2} must be positive.

- Reference rotor voltages computation

The sliding functions for the RSC voltage controllers are selected as presented in Eq. (15).

$$\begin{cases} S\left(i_{rq}\right)=i_{rq}^{c}-i_{rq}+C_{3}\int_{0}^{t}\left(i_{rq}^{c}-i_{rq}\right)d\tau \\ S\left(i_{rd}\right)=i_{rd}^{c}-i_{rd}+C_{4}\int_{0}^{t}\left(i_{rd}^{c}-i_{rd}\right)d\tau \end{cases} \tag{15}$$

$$\begin{cases} \dot{S}\left(i_{rq}\right)=\dot{i}_{rq}^{c}-\dot{i}_{rq}+C_{3}\left(i_{rq}^{c}-i_{rq}\right) \\ \dot{S}\left(i_{rd}\right)=\dot{i}_{rd}^{c}-\dot{i}_{rd}+C_{4}\left(i_{rd}^{c}-i_{rd}\right) \end{cases} \tag{16}$$

Where C_3 and C_4 must be positive gains.

The control terms $\left(v_{rd}^{c}\ \&\ v_{rq}^{c}\right)$ can be calculated by forcing $\dot{S}\left(i_{rq}\right)=0$ and $\dot{S}\left(i_{rd}\right)=0$.

$$\begin{cases} v_{rq}^{c}=\sigma.L_{r}\left(\dot{i}_{rq}^{c}+\delta.i_{rq}+\gamma.w_{r}.\psi_{sd}+w_{r}.i_{rd}+C_{3}\left(i_{rq}^{c}-i_{rq}\right)\right)+v_{rq}^{ST} \\ v_{rd}^{c}=\sigma.L_{r}\left(\dot{i}_{rd}^{c}+\alpha.i_{rd}-\beta.R_{s}.\psi_{sd}+\gamma.v_{sd}-w_{r}.i_{rq}+C_{4}\left(i_{rd}^{c}-i_{rd}\right)\right)+v_{rd}^{ST} \end{cases} \tag{17}$$

$$\begin{cases} v_{rq}^{ST}=K_{vrq}^{1}\sqrt{\left|S\left(i_{rq}\right)\right|}.sign\left(S\left(i_{rq}\right)\right)+K_{vrq}^{2}\int_{0}^{t}sign\left(S\left(i_{rq}\right)\right)d\tau \\ v_{rd}^{ST}=K_{vrd}^{1}\sqrt{\left|S\left(i_{rd}\right)\right|}.sign\left(S\left(i_{rd}\right)\right)+K_{vrd}^{2}\int_{0}^{t}sign\left(S\left(i_{rd}\right)\right)d\tau \end{cases} \tag{18}$$

Where the gains $K_{vrq}^{1},K_{vrq}^{2},K_{vrd}^{1}$ and K_{vrd}^{2} must be positive.

3.3. Integral backstepping control

The proposed control law is defined as the error between the reference value of a controlled variable and its measured value, and the integration term of this error [19].

- Reference rotor currents computation

The electromagnetic torque $\left(T_{em}\right)$ and the stator flux $\left(\psi_{sd}\right)$ tracking errors are defined as:

$$\begin{cases} Z\left(T_{em}\right)=T_{em}^{c}-T_{em}+K_{Tem}\int_{0}^{t}\left(T_{em}^{c}-T_{em}\right)d\tau \\ Z\left(\Psi_{sd}\right)=\Psi_{sd}^{c}-\Psi_{sd}+K_{\psi sd}\int_{0}^{t}\left(\Psi_{sd}^{c}-\Psi_{sd}\right)d\tau \end{cases} \tag{19}$$

$$\begin{cases} \dot{Z}\left(T_{em}\right)=\dot{T}_{em}^{c}-\dot{T}_{em}+K_{Tem}\left(T_{em}^{c}-T_{em}\right) \\ \dot{Z}\left(\Psi_{sd}\right)=\dot{\Psi}_{sd}^{c}-\dot{\Psi}_{sd}+K_{\psi sd}\left(\Psi_{sd}^{c}-\Psi_{sd}\right) \end{cases} \tag{20}$$

Where K_{Tem} and $K_{\psi sd}$ are positive parameters.

To satisfy the system stability, the Lyapunov candidate function is considered as shown in Eq. (21).

$$\begin{cases} V\left(T_{em}\right)=\frac{1}{2}Z^{2}\left(T_{em}\right) \\ V\left(\psi_{sd}\right)=\frac{1}{2}Z^{2}\left(\psi_{sd}\right) \end{cases},\ \begin{cases} \dot{V}\left(T_{em}\right)=-K_{x}.Z^{2}\left(T_{em}\right) \\ \dot{V}\left(\psi_{sd}\right)=-K_{y}.Z^{2}\left(\psi_{sd}\right) \end{cases} \tag{21}$$

Where K_{x} and K_{y} are positive gains.

The control signals of the rotor current components are inferred as follows:

$$\begin{cases} \left(i_{rq}.\psi_{sd}\right)^{c}=-\frac{1}{\mu}\left(\dot{T}_{em}^{c}+K_{Tem}\left(T_{em}^{c}-T_{em}\right)+K_{x}.Z\left(T_{em}\right)\right) \\ i_{rd}^{c}=\frac{L_{s}}{R_{s}.M}\left(\dot{\psi}_{sd}^{c}-v_{sd}+\frac{R_{s}.\psi_{sd}}{L_{s}}+K_{\psi sd}\left(\psi_{sd}^{c}-\psi_{sd}\right)+K_{y}.Z\left(\psi_{sd}\right)\right) \end{cases} \tag{22}$$

- Reference rotor voltages computation

To establish the control laws of the rotor voltages $\left(v_{rd}^{c}\ \&\ v_{rq}^{c}\right)$, let us define the rotor current errors as:

$$\begin{cases} Z\left(i_{rq}.\psi_{sd}\right)=\left(i_{rq}.\psi_{sd}\right)^{c}-\left(i_{rq}.\psi_{sd}\right)+K_{irq1}\int_{0}^{t}\left(\left(i_{rq}.\psi_{sd}\right)^{c}-\left(i_{rq}.\psi_{sd}\right)\right)d\tau \\ Z\left(i_{rd}\right)=i_{rd}^{c}-i_{rd}+K_{ird1}\int_{0}^{t}\left(i_{rd}^{c}-i_{rd}\right)d\tau \end{cases} \tag{23}$$

The Lyapunov candidate function must include the tracking errors of all previous current steps. For this, let us consider the Lyapunov function noted V_{g}.

$$V_{g}=\frac{1}{2}Z^{2}\left(T_{em}\right)+\frac{1}{2}Z^{2}\left(\psi_{sd}\right)+\frac{1}{2}Z^{2}\left(i_{rq}.\psi_{sd}\right)+\frac{1}{2}Z^{2}\left(i_{rd}\right) \tag{24}$$

$$\begin{cases} \dot{V}\left(i_{rq}.\psi_{sd}\right)=-K_{z}.Z^{2}\left(i_{rq}.\psi_{sd}\right) \\ \dot{V}\left(i_{rd}\right)=-K_{w}.Z^{2}\left(i_{rd}\right) \end{cases} \tag{25}$$

The control signals are given as mentioned in Eq. (26).

$$\begin{cases} v_{rq}^{c}=\sigma.L_{r}\left(\begin{array}{l}\frac{1}{\psi_{sd}}\left(i_{rq}.\dot{\psi}_{sd}\right)^{c}-\frac{1}{\psi_{sd}}i_{rq}.v_{sd}+\delta.i_{rq}+\gamma.w_{r}.\psi_{sd}+w_{r}.i_{rd}+\frac{R_{s}}{L_{s}}i_{rq} \\ +\frac{R_{s}.M}{L_{s}.\psi_{sd}}i_{rq}\cdot i_{rd}+\frac{K_{z}}{\psi_{sd}}Z\left(i_{rq}.\psi_{sd}\right)+\frac{K_{irq1}}{\psi_{sd}}\left(\left(i_{rq}.\psi_{sd}\right)^{c}-\left(i_{rq}.\psi_{sd}\right)\right)\end{array}\right) \\ v_{rd}^{c}=\sigma.L_{r}\left(i_{rd}^{c}+\alpha.i_{rd}-\beta.R_{s}.\psi_{sd}+\gamma.v_{sd}-w_{r}.i_{rq}+K_{ird1}\left(i_{rd}^{c}-i_{rd}\right)\right)+K_{w}.Z\left(i_{rd}\right) \end{cases} \tag{26}$$

Where K_{irq1}, K_{ird1}, K_{z} and K_{w} are chosen to be positives.

4. GSC control strategies

The objective of controlling the GSC is to keep the DC-bus voltage constant whatever the direction and the amplitude of power [13, 20]. At start-up of the WTS, the GSC brings the DC-bus voltage to the required level, after which the RSC control can be executed. The control diagram of the GSC is illustrated in Fig. 4.

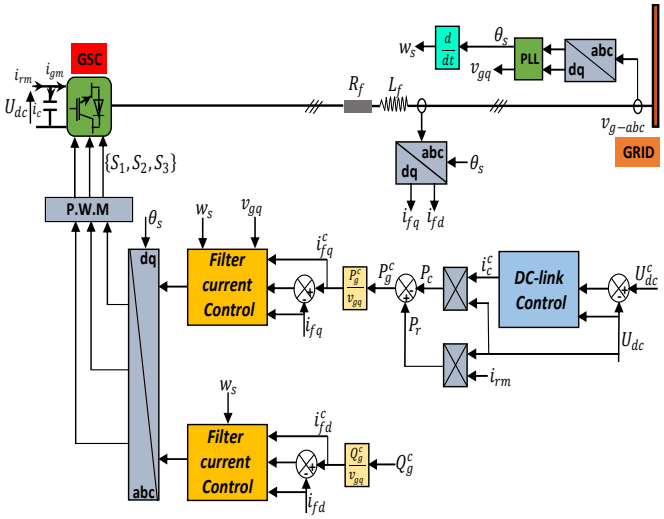

Fig. 4. GSC structure design.

The q-axis current is used to control the DC-link voltage and d-axis current to control the reactive power. The q-axis is aligned to the voltage vector. Consequently, v_{gd} becomes zero. Therefore, the active and reactive powers exchanged between the grid and the filter are expressed as given in Eq. (5), and the reference currents $\left(i_{fd}^{c}\ \&\ i_{fq}^{c}\right)$ are described in the following equations:

$$\begin{cases} i_{fq}^{c}=\frac{P_{g}^{c}}{v_{gq}} \\ i_{fq}^{c}=\frac{Q_{g}^{c}}{v_{gq}} \end{cases},\ \begin{cases} P_{q}^{c}=P_{r}^{c}-P_{c}^{c} \\ Q_{g}^{c}=0 \end{cases} \tag{27}$$

4.1. Fuzzy sliding mode control

- Filter currents control

In order to control the currents passing through the filter, the sliding surfaces are considered as follows:

$$\begin{cases} S\left(i_{fq}\right)=i_{fq}^{c}-i_{fq} \\ S\left(i_{fd}\right)=i_{fd}^{c}-i_{fd} \end{cases},\quad \begin{cases} \dot{S}\left(i_{fq}\right)=\dot{i}_{fq}^{c}-\dot{i}_{fq} \\ \dot{S}\left(i_{fd}\right)=\dot{i}_{fd}^{c}-\dot{i}_{fd} \end{cases} \tag{28}$$

Considering the following condition: $S\left(i_{fd}\right)=0$, $S\left(i_{fq}\right)=0$ and for an ideal sliding mode $\dot{S}\left(i_{fd}\right)=0$ and $\dot{S}\left(i_{fq}\right)=0$, the control components v_{fd}^{c} and v_{fq}^{c} are given as in Eq. (29).

$$\begin{cases} v_{fd}^{c}=L_f.\dot{i}_{fd}^{c}+R_f.i_{fd}-w_s.L_f.i_{fq}+v_{fd}^{fuzzy} \\ v_{fq}^{c}=L_f.\dot{i}_{fq}^{c}+R_f.i_{fq}+w_s.L_f.i_{fd}+v_{gq}+v_{fq}^{fuzzy} \end{cases} \tag{29}$$

The membership functions, for input and output variables, and the fuzzy rules used to generate the control signals are, respectively, presented in Fig. 3 and Table 1.

- DC-link voltage control

The error between the reference DC-link voltage and its actual value, which actually represents the sliding surface function, is given by Eq. (30):

$$S\left(U_{dc}\right)=U_{dc}^{c}-U_{dc}\ ,\ \dot{S}\left(U_{dc}\right)=\dot{U}_{dc}^{c}-\dot{U}_{dc} \tag{30}$$

Basing on Eq. (4) and by imposing $S\left(U_{dc}\right)=0$ and $\dot{S}\left(U_{dc}\right)=0$, so the control signal is expressed as:

$$i_{c}^{c}=C.U_{dc}^{c}+i_{c}^{fuzzy} \tag{31}$$

Symmetric triangular membership functions are defined as shown in Fig. 3, and the fuzzy rules are built by crossing such fuzzy sets as shown in Table 1.

4.2. Second order sliding mode control

- Filter currents control

Let's consider the following switching functions $S\left(i_{fq}\right)$ and $S\left(i_{fd}\right)$ for the filter currents i_{fq} and i_{fd}, respectively.

$$\begin{cases} S\left(i_{fq}\right)=i_{fq}^{c}-i_{fq}+C_5\int_0^t\left(i_{fq}^{c}-i_{fq}\right)d\tau \\ S\left(i_{fd}\right)=i_{fd}^{c}-i_{fd}+C_6\int_0^t\left(i_{fd}^{c}-i_{fd}\right)d\tau \end{cases} \tag{32}$$

$$\begin{cases} \dot{S}\left(i_{fq}\right)=\dot{i}_{fq}^{c}-\dot{i}_{fq}+C_5\left(i_{fq}^{c}-i_{fq}\right) \\ \dot{S}\left(i_{fd}\right)=\dot{i}_{fd}^{c}-\dot{i}_{fd}+C_6\left(i_{fd}^{c}-i_{fd}\right) \end{cases} \tag{33}$$

Where C_5 and C_6 must be positive.

Letting $S\left(i_{fd}\right)=S\left(i_{fq}\right)=0$ and $\dot{S}\left(i_{fd}\right)=\dot{S}\left(i_{fq}\right)=0$, the control signals v_{fd}^{c} and v_{fq}^{c} can be simply retrieved.

$$\begin{cases} v_{fd}^{c}=L_f.\dot{i}_{fd}^{c}+R_f.i_{fd}-w_s.L_f.i_{fq}+C_6\left(i_{fd}^{c}-i_{fd}\right) \\ v_{fq}^{c}=L_f.\dot{i}_{fq}^{c}+R_f.i_{fq}+w_s.L_f.i_{fd}+v_{gq}+C_5\left(i_{fq}^{c}-i_{fq}\right) \end{cases} \tag{34}$$

$$\begin{cases} v_{fd}^{ST}=K_{vfd}^{1}\sqrt{\left|S\left(i_{fd}\right)\right|}.sign\left(S\left(i_{fd}\right)\right)+K_{vfd}^{2}\int_0^t sign\left(S\left(i_{fd}\right)\right)d\tau \\ v_{fq}^{ST}=K_{vfq}^{1}\sqrt{\left|S\left(i_{fq}\right)\right|}.sign\left(S\left(i_{fq}\right)\right)+K_{vfq}^{2}\int_0^t sign\left(S\left(i_{fq}\right)\right)d\tau \end{cases} \tag{35}$$

With: K_{vfd}^{1}, K_{vfd}^{2}, K_{vfq}^{1} and K_{vfq}^{2} are chosen positives.

- DC-link voltage control

Using the same principle of STA presented previously, the switching function of DC-link voltage error is defined by the following relationship:

$$\begin{cases} S\left(U_{dc}\right)=U_{dc}^{c}-U_{dc}+C_c\int_0^t\left(U_{dc}^{c}-U_{dc}\right)d\tau \\ \dot{S}\left(U_{dc}\right)=\dot{U}_{dc}^{c}-\dot{U}_{dc}+C_c\left(U_{dc}^{c}-U_{dc}\right) \end{cases} \tag{36}$$

Thus, the control signal is given as depicted in Eq. (37):

$$\begin{aligned} i_{c}^{c}=&C\left(\dot{U}_{dc}^{c}+C_c\left(U_{dc}^{c}-U_{dc}\right)\right)+K_{ic}^{1}\sqrt{\left|S\left(U_{dc}\right)\right|}.sign\left(S\left(U_{dc}\right)\right) \\ &+K_{ic}^{2}\int_0^t sign\left(S\left(U_{dc}\right)\right)d\tau \end{aligned} \tag{37}$$

C_c, K_{ic}^{1}, and K_{ic}^{2} are positive gains.

4.3. Integral backstepping control

- Filter currents control

To design the control inputs v_{fd}^{c} and v_{fq}^{c}, the following filter current tracking errors are introduced.

$$\begin{cases} Z\left(i_{fq}\right)=i_{fq}^{c}-i_{fq}+K_{ifq}\int_0^t\left(i_{fq}^{c}-i_{fq}\right)d\tau \\ Z\left(i_{fd}\right)=i_{fd}^{c}-i_{fd}+K_{ifd}\int_0^t\left(i_{fd}^{c}-i_{fd}\right)d\tau \end{cases} \tag{38}$$

$$\begin{cases} \dot{Z}\left(i_{fq}\right)=\dot{i}_{fq}^{c}-\dot{i}_{fq}+K_{ifq}\left(i_{fq}^{c}-i_{fq}\right) \\ \dot{Z}\left(i_{fd}\right)=\dot{i}_{fd}^{c}-\dot{i}_{fd}+K_{ifd}\left(i_{fd}^{c}-i_{fd}\right) \end{cases} \tag{39}$$

The Lyapunov functions associated, respectively, to i_{fq} and i_{fd} errors are given as presented in Eq. (40):

$$\begin{cases} V\left(i_{fq}\right)=\frac{1}{2}Z^{2}\left(i_{fq}\right) \\ V\left(i_{fd}\right)=\frac{1}{2}Z^{2}\left(i_{fd}\right) \end{cases},\quad \begin{cases} \dot{V}\left(i_{fq}\right)=-K_f^{1}.Z^{2}\left(i_{fq}\right) \\ \dot{V}\left(i_{fd}\right)=-K_f^{2}.Z^{2}\left(i_{fd}\right) \end{cases} \tag{40}$$

Therefore, the control signals are deduced as given in Eq. (41):

$$\begin{cases} v_{fd}^{c} = L_f.\dot{i}_{fd}^{c} + R_f.i_{fd} - w_s.L_f.i_{fq} + K_{ifd}\left(i_{fd}^{c} - i_{fd}\right) + K_f^1.Z\left(i_{fd}\right) \\ v_{fq}^{c} = L_f.\dot{i}_{fq}^{c} + R_f.i_{fq} + w_s.L_f.i_{fd} + v_{gq} + K_{ifq}\left(i_{fq}^{c} - i_{fq}\right) + K_f^2.Z\left(i_{fq}\right) \end{cases} \quad (41)$$

Where K_{ifd}, K_{ifq}, K_f^1 and K_f^2 must be positive.

- DC-link voltage control

The DC-link voltage error $Z\left(U_c\right)$ is defined by Eq. (42):

$$\begin{cases} Z\left(U_{dc}\right) = U_{dc}^{c} - U_{dc} + K_{dc}\int_0^t \left(U_{dc}^{c} - U_{dc}\right)d\tau \\ \dot{Z}\left(U_{dc}\right) = \dot{U}_{dc}^{c} - \dot{U}_{dc} + K_{dc}\left(U_{dc}^{c} - U_{dc}\right) \end{cases} \quad (42)$$

Based on Eq. (4) and the Lyapunov candidate function given in Eq. (43), which should be carefully chosen, the control law of the capacitor current is illustrated by the following relationship:

$$\begin{cases} V\left(U_{dc}\right) = \frac{1}{2}Z^2\left(U_{dc}\right), \dot{V}\left(U_{dc}\right) = -K_{dc}^1.Z^2\left(U_{dc}\right) \\ i_c^{c} = C\left(\dot{U}_{dc}^{c} + K_{dc}\left(U_{dc}^{c} - U_{dc}\right) + K_{dc}^1.Z\left(U_{dc}\right)\right) \end{cases} \quad (43)$$

With K_{dc} and K_{dc}^1 are positive gains.

5. Simulation results and Discussion

The simulation test aim is to apply a variable wind speed profile in order to emulate an efficient wind turbulence. The wind profile is chosen as a ramp varies between 9 and 11.5 m/s (Fig. 5) to give a various operating modes (sub-synchronous and super-synchronous). The SMC, BS, FSM, IBS and SOSM controllers ensure the tracking of the maximum power point (MPPT), and this, by keeping λ to an optimum value $\left(\lambda_{opt} = 7.8\right)$ and C_p to its maximum value $\left(C_{p-\max} = 0.438\right)$ as illustrated in Fig. 6. A high efficiency of the captured power and smooth tracking with a neglected mechanical stress are actually expected, as the DFIG's electromagnetic torque variations are minimal, due to a non-abrupt change of the operating point. The mechanical speeds follow its reference almost perfectly for the used controllers (except the SMC that introduced the chattering phenomenon) as shown in Fig. 7. The control strategy intervenes and β values increase, vary between 0◦ and 90◦ ($\lambda < \lambda_{opt}$, the operating point is at the left side of the $C_{p-\max}$ curve) as illustrated in Fig. 8, in such a way as to protect the WTS against any overload or destruction.

Figure 9, Fig. 10, Fig. 11 and Fig. 12 show the simulation results of the electromagnetic torque, the stator flux and the stator active and reactive power, respectively. The measured values track their desired values with different efficiency. The stator active power (Fig. 11) depends on the electromagnetic torque (Fig. 9), that is itself depends on the wind speed variation, and this can be translated by its identical form of the T_{em} waveform. Therefore, the P_s is a consequence of T_{em}. The stator reactive power is forced to be around zero in such way to allow the DFIG operating with a unity power factor as illustrated in Fig. 14. Figure 13 illustrates the DC-bus voltage (U_{dc}) curves of the proposed controllers and it can be seen that the capacitor voltage remains stabilized.

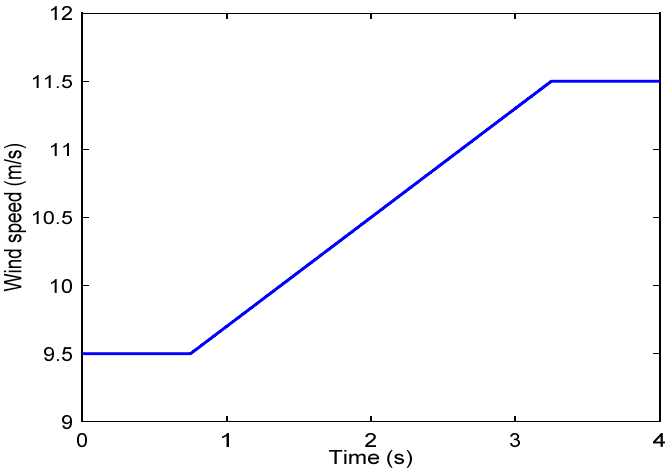

Fig. 5. Wind variation profile

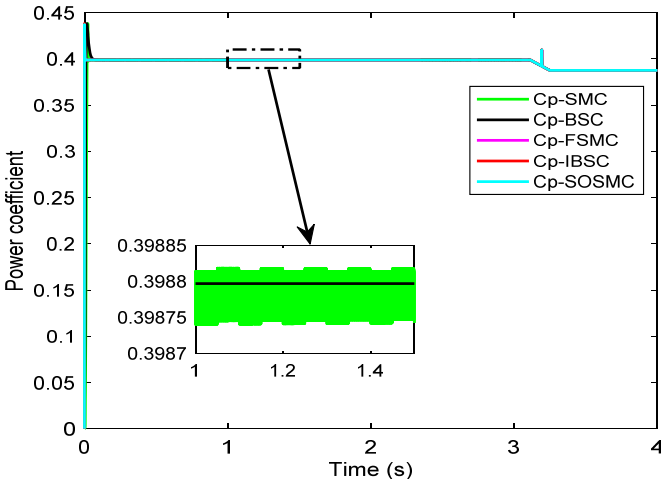

Fig. 6. Efficiency coefficient

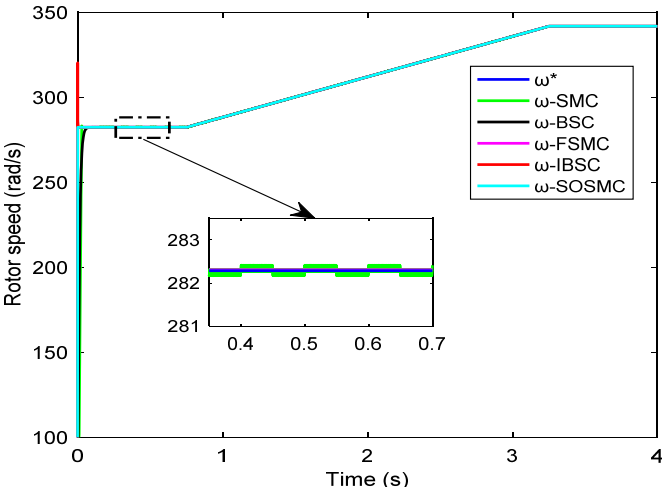

Fig. 7. Mechanical speed of the DFIG

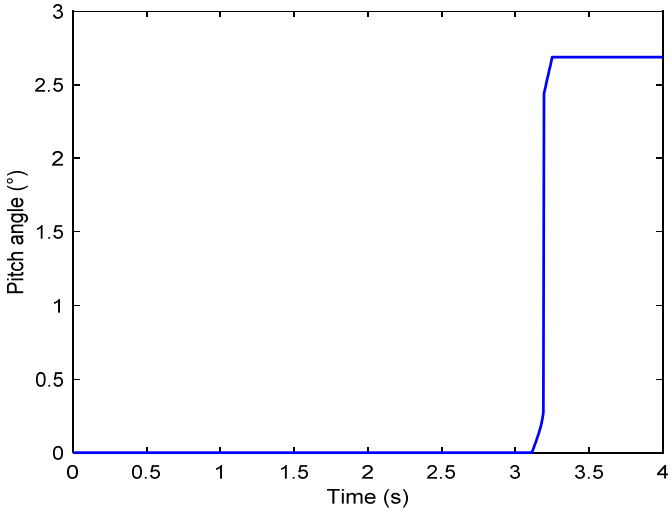

Fig. 8. Pitch angle variation

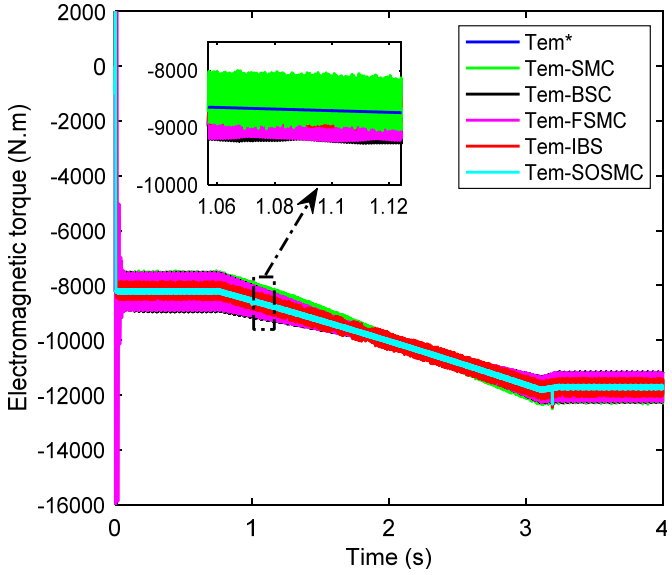

Fig. 9. Electromagnetic torque of the DFIG

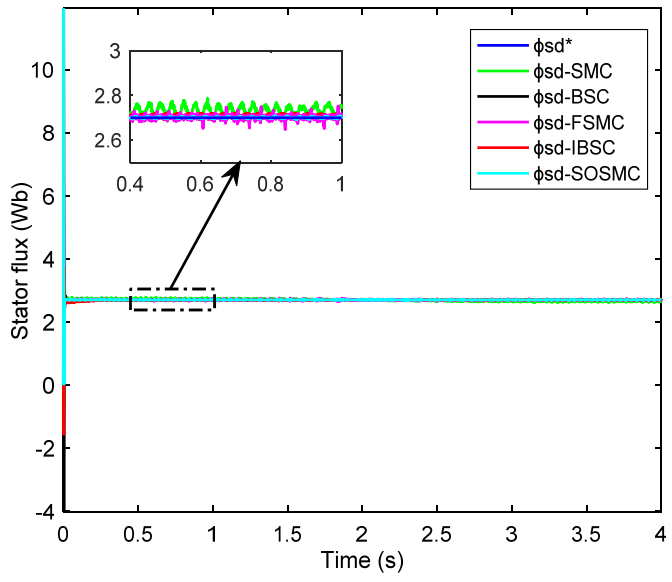

Fig. 10. Stator flux

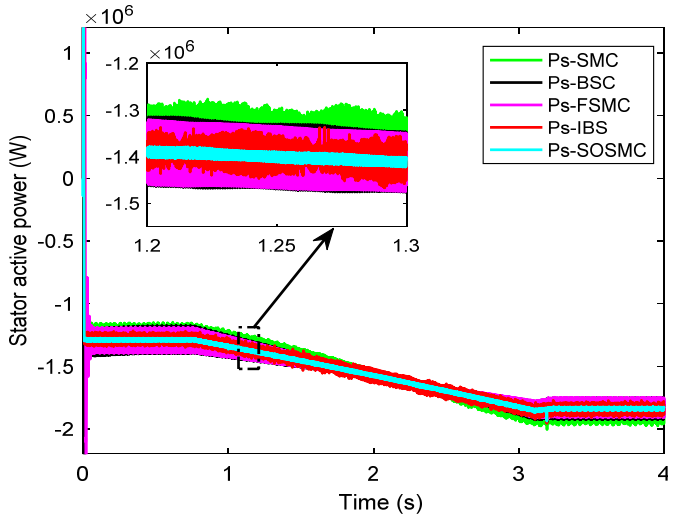

Fig. 11. Stator active power

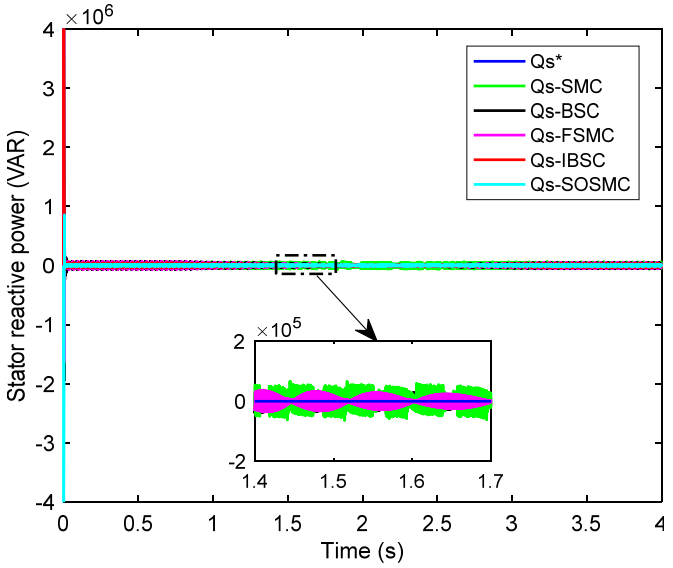

Fig. 12. Stator reactive power

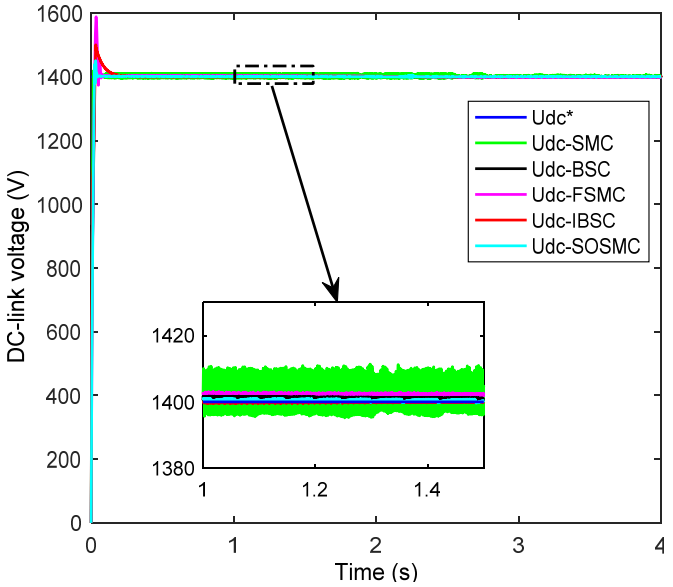

Fig. 13. DC-bus voltage

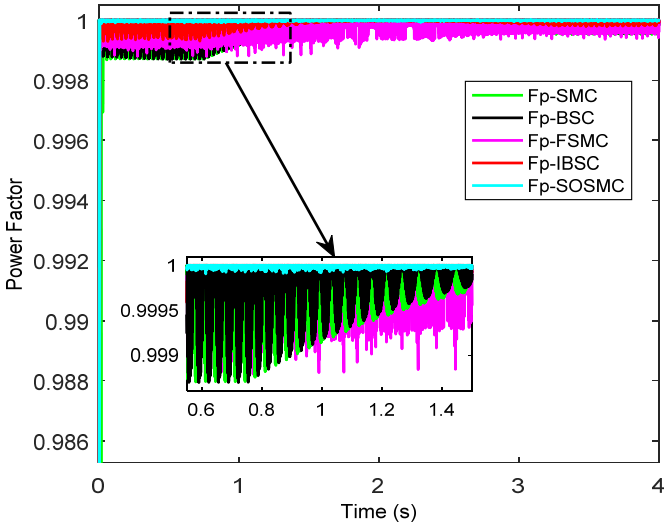

Fig. 14. Power factor

Based on simulation results, we can conclude that the decoupling control of the d-axis and q-axis; and the tracking performances are achieved of all the methods. Apparently, there is no-significant difference between them. It is evident to see less chattering in the curves of the controlled variables with BSC, FSMC, IBSC and SOSMC methods than the SMC method, because these controllers do not contain the discontinuous component. Actually, all the methods (SMC, BSC, FSMC, IBSC and SOSMC) could regulate well the electromagnetic torque (Fig. 9), stator flux (Fig. 10), active and reactive powers (Fig. 11 and Fig. 12) and DC-link voltage (Fig. 13) where no sudden oscillations, no peak and no overshoot observed in the electrical variable (T_{em}, ψ_{sd}, P_s, Q_s and U_{dc}) waveforms. Nevertheless, the SMC, BSC and FSMC present a remarkable ripples especially in the electromagnetic torque and stator powers. These ripples decrease as long as the slip angular speed becomes around zero. On the other hand, the IBSC and SOSMC control scheme have low ripples and neglected steady state error, and this is due to the integral term, moreover, the SOSMC presents a fast dynamic responses, less ripples and less steady state error than the IBSC.

6. Robustness against parameters variations

In this work, as a first step, R_s, R_r, R_f and C are increased by ζ, while L_s, L_r, L_f and M are decreased by θ, respectively. As a second step, the resistances and capacitance are increased by η, while the proper and mutual inductances are decreased by γ, respectively. The attenuation/enlargement parameters ζ, θ, η, γ are chosen to be equal to 1.8, 0.2, 1.5, 0.5, respectively. Figure 15, Fig. 16 and Fig. 17 show the simulation results.

The results depicted in Fig. 15, Fig. 16 and Fig. 17 shown that the electromagnetic torque, stator flux and DC-bus voltage responses with SOSM controller remain outstandingly insensible to the variation of the resistances, capacitance and magnetizing inductances simultaneously. This is due its high ability to reject the parameter uncertainties, i.e., ST algorithm do not depend on the system parameters, such as that the highest robustness can be achieved.

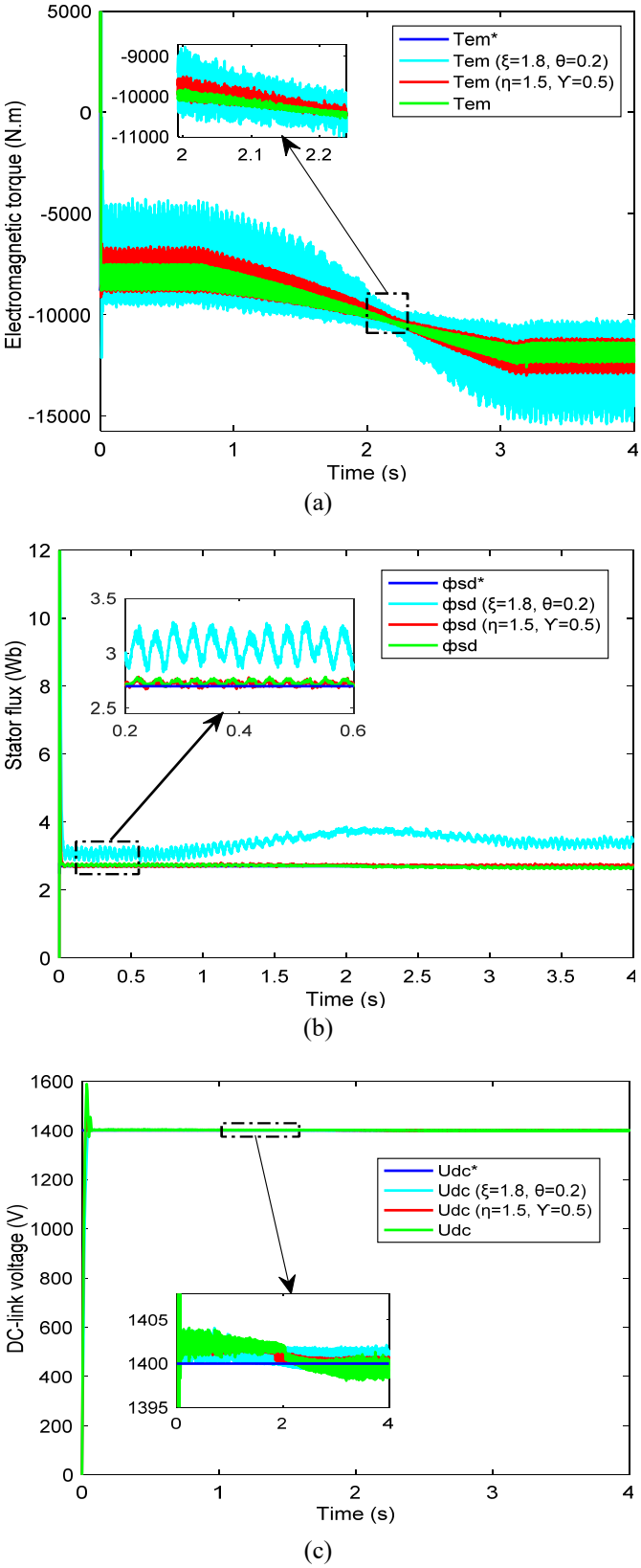

Fig. 15. FSMC strategy responses under parameters variations: (a) Electromagnetic torque (b) Stator flux (c) DC-link voltage

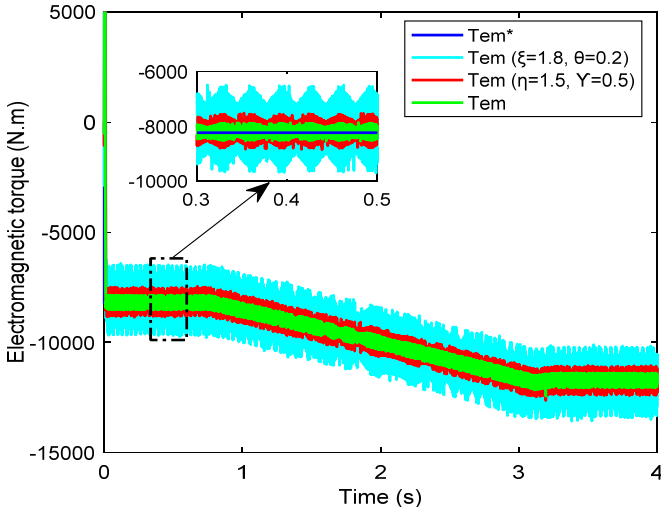

(a)

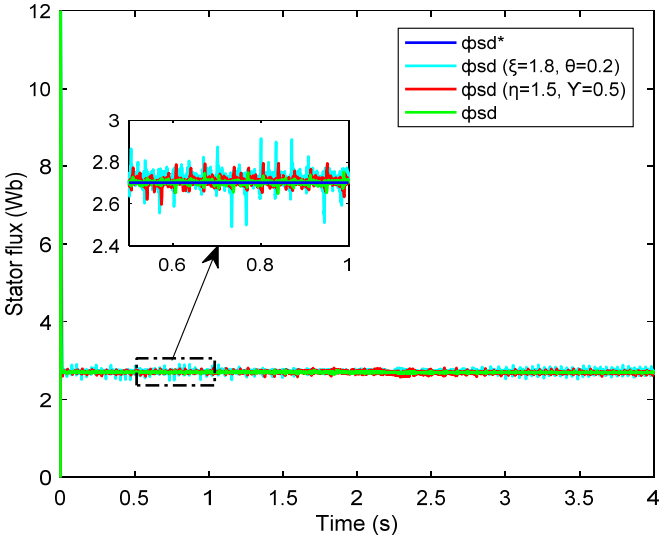

(b)

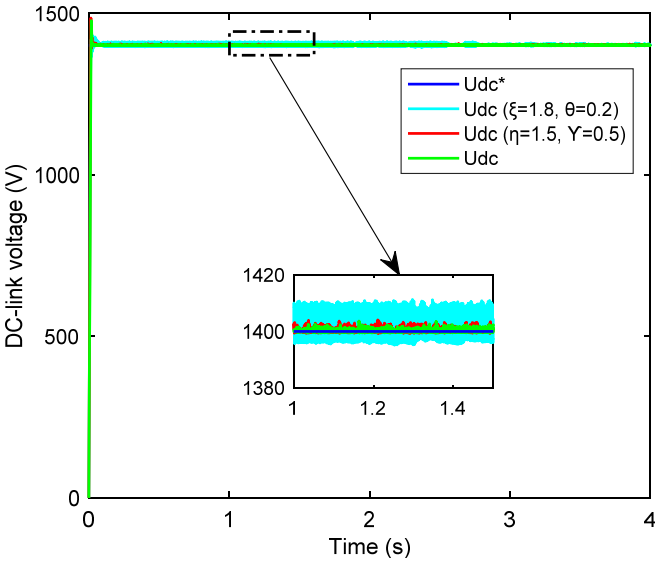

(c)

Fig. 16. IBSC strategy responses under parameters variations: (a) Electromagnetic torque (b) Stator flux (c) DC-link voltage

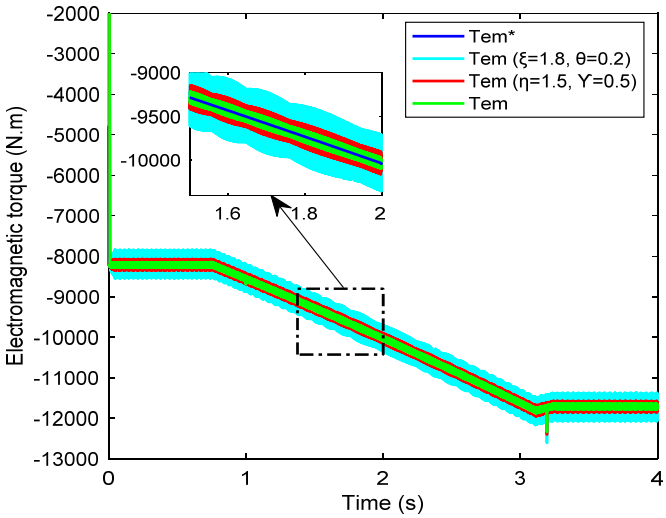

(a)

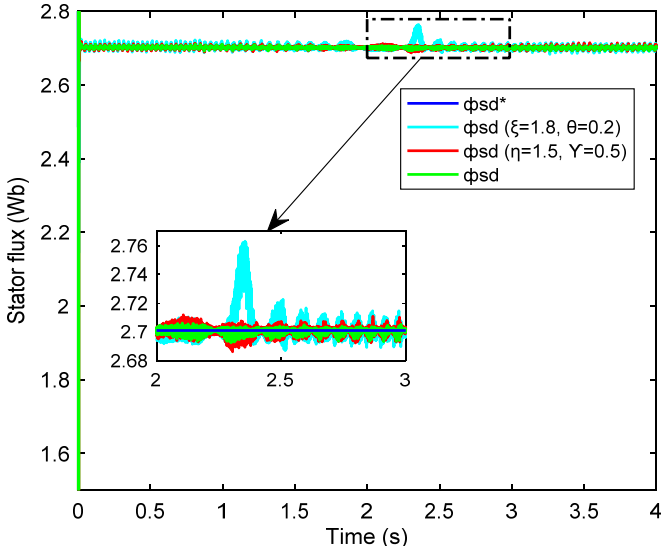

(b)

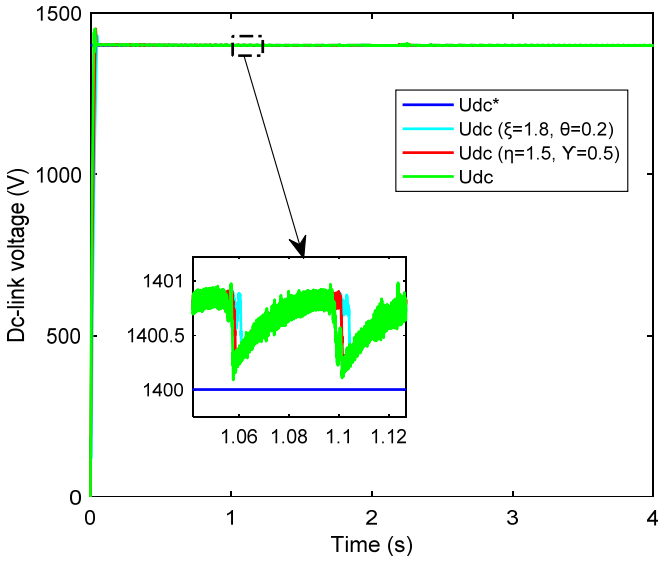

(c)

Fig. 17. SOSMC strategy responses under parameters variations: (a) Electromagnetic torque (b) Stator flux (c) DC-link voltage

7. Conclusions and Suggestions

This work describes a comparative study between different control schemes of WECS based on DFIG. The proposed methods have been applied to both PWM converters: RSC and GSC. The performance of the proposed control strategies have been investigated where the DFIG's speed and parameters intentionally changed. These changes yield to significant disturbances on the stator flux and electromagnetic torque waveforms for FSM control technique, while these effects are almost neglected for a system with SOSM controller. Similarly, the inherent robustness of IBS controller is enhanced by the integral term. The described SOSMC approach delivers exceedingly satisfactory performances in term of tracking and ability to reject the influence of the DFIG's speed and parameters variation. Furthermore, the SOSMC method removes the chattering phenomenon characterizing the classical SMC. Compared to other nonlinear approaches, SOSMC can be a very beneficial solution for WECS based on DFIG, despite its complexity in the industry. With an adequate choice of the controller's gains, the proposed methods will ensure more robustness and highest quality of the simulation results. In some cases, the grid is undergoing a voltage dip that can cause large damage even if it is relatively low.

Our future work will be focused on the examination of robustness of the proposed control strategies under unbalanced voltage conditions. In addition, the optimization of the controller's gains will also be introduced in order to reach a better results.

Appendix

Table 2. WECS parameters

Nominal power P_s	2 MW
Rated stator voltage V_s	400 V
Stator resistance R_s	0.0026 Ω
Rotor resistance R_r	0.0029 Ω
Stator inductance L_s	0.002587 H
Rotor inductance L_r	0.002587 H
Mutual inductance M	0.0025 H
Moment of inertia J	890 Kg.m^2
Grid Frequency f_s	50 Hz
Friction coefficient f	0.1 N.m.s/rad
Blade radius R	42 m
Gearbox gain G	80
Filter resistance R_f	0.075 Ω
Filter inductance L_f	0.00075 mH
DC-link capacitor C	0.038 F
DC-link voltage U_{dc}	1400 V

Acknowledgements

This work has been supported by National Center for Scientific and Technical Research (CNRST), Rabat, Morocco.

References

[1]M. Doumi, A. G. Aissaoui, M. Abid, I. Colak, and A. Tahour. "Robust MRAC For A Wind Turbine Based On A Doubly-Fed Induction Generator", 6th International Conference on Renewable Energy Research and Applications, San Diego, CA, USA, 5-8 November 2017. (Conference Paper)

[2]M. Fdaili, A. Essadki, T. Nasser, "Comparative Analysis Between Robust SMC & Conventional PI Controllers Used in WECS Based on DFIG". IJRER, Vol. 7, pp. 2151-2161, 2017. (Article)

[3]M. Nadour, A. Essadki, M. Fdaili, T. Nasser, "Advanced Backstepping Control of a Wind Energy Conversion System Using a Doubly-Fed Induction Generator", 5th International Renewable and Sustainable Energy Conference (IRSEC), Tangier, Morocco, 4-7 December 2017. (Conference Paper)

[4]M. Achglaf, C. Nichita, B. Dakyo, "Control Strategies Design for a Small-Scale Wind Turbine with a Doubly Fed Induction Generator", 7th International Conference on Renewable Energy Research and Applications, Paris, France, 14-17 October 2018. (Conference Paper)

[5]R. V. Jacomini, J. Alfeu, S. Filho, "Direct Power Control Strategy to Enhance the Dynamic Behavior of DFIG During Voltage Sag", 7th International Conference on Renewable Energy Research and Applications, Paris, France, 14-17 October, 2018. (Conference Paper)

[6]K, Boulaam, A. Boukhelifa. "Fuzzy Sliding Mode Control of DFIG Power for a Wind Conversion System". 16th International Power Electronics and Motion Control Conference and Exposition, Antalya, Turkey, 21-24 September, 2014. (Conference Paper)

[7]S. Ardjoun, M. Abid, "Fuzzy sliding mode control applied to a doubly fed induction generator for wind turbines". Turkish J Electr Eng Comput Sci, Vol. 23, pp. 1673-1686, 2015. (Article)

[8]G. Zoubir, B. Cheikh, A. Tayeb, B. Belkacem, "Speed-Sensorless DFIG Wind Turbine for Power Optimization Using Fuzzy Sliding Mode Observer", IJRER, Vol. 7, No. 2, pp. 613-621, 2017. (Article)

[9]A. Damiano, GL. Gatto, I. Marongiu, A. Pisano, "Second-order sliding-mode control of dc drives", IEEE Trans Ind Electron, Vol. 51, pp- 364-373, 2004. (Article)

[10]I. Guenoune, F. Plestan, A. Chermitti, "Control of a New Structure of twin wind turbine", 5th International Conference on Renewable Energy Research and Applications, Birmingham, UK, 20-23 November 2016. (Conference Paper)

[11]M. Hoshyar, M. Mola, "Full Adaptive Integral Backstepping Controller for Interior Permanent Magnet

Synchronous Motors". Asian J Control, Vol. 20, pp. 1-12, 2017. (Article)

[12]Z. Boudjema, R. Taleb, E. Bounadja, "A new robust control scheme using second order sliding mode and fuzzy logic of a DFIM supplied by two five-level SVPWM inverters", AIP Conference Proceedings, pp. 1-15, 2017. (Conference Paper)

[13]I. Kharchouf, A. Essadki, M. Arbaoui, T. Nasser, "Modeling and PI Control Strategy of DFIG Based Wind Energy Conversion Systems", 5th International Renewable and Sustainable Energy Conference (IRSEC), Tangier, Morocco, 4-7 December 2017. (Conference Paper)

[14]R. D. Shukla, R. K. Tripathi, "Instantaneous direct voltage and frequency control in DC grid tied DFIG based wind energy system", Electrical Power and Energy Systems, Vol. 100, pp. 309-319, 2018. (Article)

[15]Y. C. liu, S. Laghrouche, A. N'Diaye, M. Cirrincione. "Active-Flux-Based Super-Twisting Sliding Mode Observer for Sensorless Vector Control of Synchronous Reluctance Motor Drives", 7th International Conference on Renewable Energy Research and Application, Paris, France, 14-17 October 2018. (Conference Paper)

[16]B. Meghni, D. Dib, AT. Azar, "A second-order sliding mode and fuzzy logic control to optimal energy management in wind turbine with battery storage", Neural Comput & Appl, Vol. 28, pp. 1417-1438, 2017. (Article)

[17]A. Levant, "High-order sliding modes, differentiation and output-feedback control". Int J Control, Vol. 76, pp. 924-941, 2003. (Article)

[18]A. Levant, L. Alelishvili, "Integral High-Order Sliding Modes", IEEE TRANSACTIONS ON AUTOMATIC CONTROL, Vol. 52, pp. 1278-1282, 2007. (Article)

[19]O. Adekanle, M. Guisser, E. Abdelmounim, M. Aboulfatah, "Integral Backstepping controller combined with High Gain Observer for the optimization of grid-connected Doubly-Fed Induction Generator", International Conference on Wireless Technologies, Embedded and Intelligent Systems (WITS), Fez, Morocco, 19-20 April 2017. (Conference Paper)

[20]A. Dida, D. Benattous, "A complete modeling and simulation of DFIG based wind turbine system using fuzzy logic control", Front Energy, Vol. 10, pp. 143-154, 2016. (Article)